Svedberg Open
DISSEMINATIONOFKNOWLEDGE

International Journal of Artificial Intelligence and Machine Learning

Publisher's Home Page: https://www.svedbergopen.com/



Research Paper Open Access

# Comparative Multi-Objective Optimization Strategies for Intelligent Energy Management of Grid-Connected Microgrids Using BILSTM Forecasting

Yacine Ahmouda[1], Boussaid Ouzine[2], Mohamed Nacer Saadi[2], Mohamed Moustafa Bouzaki[3], Abdelghani Yahiou [4], Samia Bouzouaid [5], Abdelkader Laafer [6]

[1] Research Laboratory of Industrial Risk, Non-Destructive Control and Operating Safety, Badji Mokhtar Annaba University, B.P. 12, Annaba, Algeria. Email: yacine.ahmouda@univ-annaba.dz .
[2] Research Laboratory of Industrial Risk, Non-Destructive Control and Operating Safety, Badji Mokhtar Annaba University, B.P. 12, Annaba, Algeria. Email :ouzine.boussaid@univ-annaba.dz, Email mohamednacer.saadi@univ-annaba.dz
[3] Department Renewable Energy, University of Blida 1, Algeria. Email:Bouzaki.mohamed@univ-blida.dz
[4] Department of Electrical Engineering, Faculty of Technology, University of Sétif 1, Sétif, Algeria. Email:abdelghani.yahiou@univ-bouira.dz
[5] Department of Civil Engineering and Hydraulic of Applied Sciences, Laboratory of Exploitation and Valorization of Natural Resources in Arid Zones, University Kasdi Merbah Ouargla, Ouargla, Algeria. Email:bouzouaid.samia@univ-ouargla.dz
[6] University of Blida 1, Institute of Architecture and Urbanism, Ovamus Laboratory, Blida 09000, Algeria. Email:a.laafer@univ-blida.dz

Received: 30/06/2026 Accepted: 17/10/2026 Published: 25/10/2026

**ABSTRACT**

This paper presents a comparative multi-objective optimization framework for intelligent energy management of a grid-connected microgrid integrating photovoltaic generation, battery energy storage, and bidirectional grid interaction. A Bidirectional Long Short-Term Memory (BiLSTM) neural network is employed to accurately forecast load demand and photovoltaic power generation using realistic meteorological and operational data. The predicted profiles are subsequently integrated into a multi-objective Energy Management System (EMS) formulated over a 24-hour scheduling horizon. The EMS optimization problem simultaneously minimizes electricity operating cost and battery utilization while satisfying battery State of Charge (SOC) limits and grid operational constraints. Three multi-objective optimization algorithms, namely Non-dominated Sorting Genetic Algorithm II (NSGA-II), Multi-Objective Particle Swarm Optimization (MOPSO), and Adaptive Multi-Objective Particle Swarm Optimization (AMOPSO), are comparatively evaluated for optimal battery scheduling. Simulation results demonstrate that the considered optimization algorithms exhibit different trade-offs between economic performance and battery utilization. MOPSO achieves the lowest electricity operating cost due to its strong exploitation capability, whereas NSGA-II provides improved Pareto front diversity and exploration performance. AMOPSO offers stable convergence behavior and balanced operating solutions. The comparative analysis highlights the strengths and limitations of each optimization strategy in the context of intelligent microgrid energy management. The obtained results confirm that combining BiLSTM forecasting with multi-objective optimization provides an effective framework for improving energy scheduling, battery management, and operational flexibility in grid-connected microgrids.

**Index Terms:** Renewable Energy, Battery, Energy Management System, Microgrid, BiLSTM, Multi-objective Optimization, Storage.

## I. Introduction

The increasing integration of renewable energy sources into modern power systems has strengthened the role of microgrids as a practical means of combining local generation, energy storage, flexible loads, and interaction with the utility grid [1], [2]. Photovoltaic (PV) generation is particularly attractive because of its relatively mature technology and broad deployment potential. Its intermittent nature, however, introduces fluctuations in power availability that can complicate the balance between generation and demand [3], [4]. These fluctuations become more difficult to manage when PV generation is combined with industrial loads whose demand may change considerably over relatively short periods.

Battery energy storage systems (BESSs) provide an effective means of dealing with this variability. They can absorb surplus PV energy and release it when renewable production is insufficient, thereby giving the microgrid additional operational flexibility [5], [6]. The benefit of storage nevertheless depends on how it is scheduled. Frequent or unnecessarily large charging and discharging actions may increase battery degradation, while conservative operation can lead to greater reliance on grid electricity. The coordination of PV generation, BESS operation, load demand, and grid exchange therefore results in a constrained optimization problem in which

economic operation must be considered together with battery usage [7]. This issue is particularly relevant to industrial microgrids, where load variations and peak-demand periods can have a direct impact on operating costs [8].

Energy management systems (EMSs) are consequently responsible for determining how the available resources should be operated while respecting the physical and operational limits of the microgrid [9], [10]. Rule-based strategies remain attractive because of their simplicity, but their predefined operating rules may become restrictive when system conditions change rapidly or when several conflicting objectives have to be considered [11]. Optimization-based EMSs provide greater flexibility because they can incorporate operational constraints directly into the scheduling problem and evaluate trade-offs between competing objectives [12]. In a multi-objective formulation, for example, reducing electricity cost may require battery actions that are not necessarily favorable from the perspective of degradation. The resulting Pareto set can therefore provide several feasible compromises rather than a single operating solution [13-15].

A number of evolutionary and swarm-based algorithms have been investigated for this type of problem. NSGA-II has become a widely used benchmark because of its non-dominated sorting procedure and its mechanism for maintaining solution diversity [16]. MOPSO offers a different search mechanism based on particle interactions and has also been applied extensively to multi-objective energy management problems [17]. Adaptive versions such as AMOPSO modify the search behavior during optimization and have been considered for constrained microgrid applications [18]. Although these approaches share the same general objective, their search mechanisms can lead to different convergence characteristics, Pareto-front distributions, and computational behavior. Comparing them under a common experimental setting is therefore useful when the objective is not simply to introduce another optimizer, but to understand how different optimization strategies perform for the same EMS problem.

The quality of the optimization, however, is also linked to the information supplied to the scheduling process. In a look-ahead EMS, decisions for the coming hours depend on estimates of future load and renewable generation. Errors in these forecasts can consequently propagate into the optimization stage and modify the resulting battery and grid schedules [19–21]. This has encouraged the use of machine-learning and deep-learning models for short-term energy forecasting, particularly when the underlying data contain nonlinear temporal relationships [22–24]. LSTM networks are well suited to this type of problem because they can retain information over extended sequences and have been widely used for load and renewable-energy forecasting [25]. BiLSTM networks extend this structure by processing temporal patterns in both directions, allowing the model to use contextual information from the complete input sequence [26], [27]. Their use is therefore relevant to a forecasting stage that must provide load and PV trajectories to a subsequent EMS optimization process.

Despite the substantial body of work on forecasting and microgrid optimization, these two components are still frequently investigated independently. Studies that combine forecasting with optimization do not always provide a direct comparison of several multi-objective algorithms under the same data, objective functions, and operational constraints [28–30]. This makes it difficult to determine whether differences in reported results arise from the optimization method itself or from differences in the experimental setup. The issue is particularly relevant for industrial microgrids operating under demanding environmental conditions, where both renewable variability and battery operating conditions can affect the quality of the resulting schedule. The Hassi Messaoud region in southern Algeria provides an appropriate context for such an investigation because of its strong solar resource and its harsh Saharan climate [31-34]. These characteristics make the region attractive for PV-based generation while also creating practical challenges for the operation and long-term use of energy storage systems.

Against this background, this study develops an intelligent EMS for a grid-connected industrial microgrid composed of PV generation, a BESS, electrical loads, and the utility grid [35]. The proposed framework combines multivariate BiLSTM forecasting of PV power and electrical demand with a multi-objective scheduling layer operating over a 24-hour horizon. Rather than focusing on the development of a new optimization algorithm, the study places particular emphasis on a controlled comparison of three established approaches, namely NSGA-II, MOPSO, and AMOPSO. The comparison is conducted under the same operating conditions and within the same EMS formulation, with the aim of examining their respective capabilities in balancing electricity cost and battery degradation.

The main contribution of this work lies in the integration of short-term multivariate forecasting and degradation-aware multi-objective energy management within a common framework for a grid-connected industrial microgrid. The BiLSTM model simultaneously forecasts PV generation and electrical load using meteorological, electrical, and economic variables representative of the Hassi Messaoud operating context. These forecasts are then incorporated into the EMS scheduling process, where electricity operating cost and battery degradation are considered simultaneously while satisfying power-balance, battery state-of-charge, and grid operating constraints. In addition, the study provides a controlled comparison of NSGA-II, MOPSO, and AMOPSO using identical initial conditions and the same optimization formulation. Their behavior is examined through complementary indicators describing convergence, Pareto-front diversity and spacing, hypervolume, stability, and the resulting energy-management performance. This comparative setting is intended to provide a more consistent basis for assessing the practical differences between the three optimization strategies rather than assuming the superiority of one method in advance.

The remainder of this paper is organized as follows. Section II presents the microgrid architecture and its

mathematical model. Section III describes the data generation process and the BiLSTM forecasting methodology. Section IV formulates the multi-objective EMS problem and describes the three optimization algorithms considered in the comparison. Section V presents and discusses the simulation results, including the Pareto fronts and comparative performance indicators. Section VI concludes the paper and discusses possible directions for future work.

## II. MICROGRID SYSTEM DESCRIPTION

### A. Architecture of the Proposed Intelligent EMS Framework

The proposed intelligent Energy Management System (EMS) framework combines advanced forecasting and multi-objective optimization techniques to improve the operational performance of a grid-connected microgrid integrating photovoltaic (PV) generation, battery energy storage, and utility grid interaction. The overall architecture of the proposed framework is illustrated in Fig. 1.

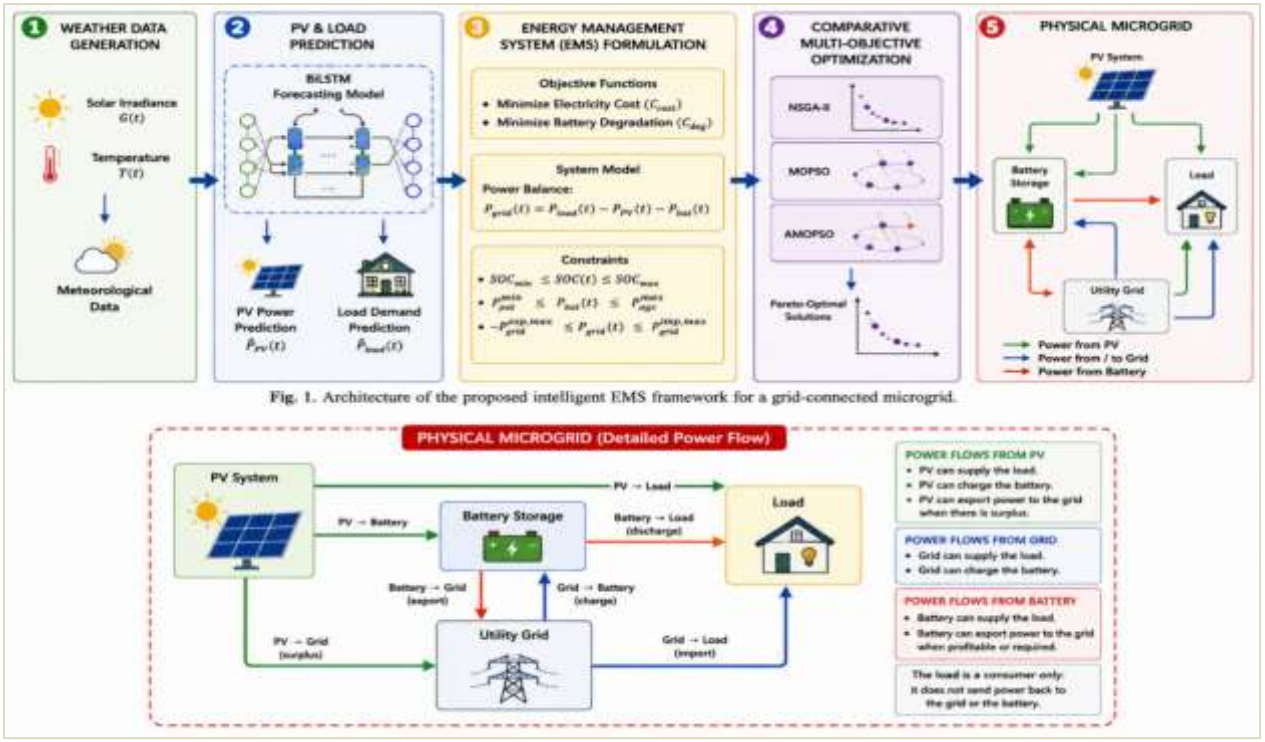



Fig. 1. Architecture of the proposed intelligent EMS framework for a grid-connected microgrid.

**Fig. 1. Architecture of the proposed intelligent EMS framework**

As illustrated in Fig. 1, the proposed intelligent EMS framework is composed of five interconnected functional blocks: weather data generation, PV and load prediction, energy management system formulation, comparative multi-objective optimization, and the physical microgrid.

The first block generates the meteorological variables required for photovoltaic power forecasting, including solar irradiance and ambient temperature. These data, together with historical load demand information, are supplied to the second block, which employs a Bidirectional Long Short-Term Memory (BiLSTM) neural network to predict both photovoltaic generation and load demand over a 24-hour scheduling horizon.

The forecasted profiles are subsequently transferred to the Energy Management System (EMS) block, where the microgrid operation is formulated as a constrained multi-objective optimization problem. The EMS aims to determine the optimal battery charging/discharging schedule and the optimal power exchange with the utility grid while satisfying all operational constraints.

### B. Microgrid System Description

The physical microgrid considered in this study corresponds to Block 5 of the proposed intelligent EMS framework illustrated in Fig. 1. This block represents the real operating environment in which the optimal control decisions generated by the Energy Management System (EMS) are applied. The microgrid consists of four main components: a photovoltaic (PV) generation system, a battery energy storage system (BESS), local electrical loads, and a utility grid connection.

The operation of the microgrid relies on the coordinated exchange of energy among these components. Depending on the operating conditions, the photovoltaic generation can directly supply the electrical load, charge the battery storage system, or export surplus energy to the utility grid. Similarly, the battery energy storage system can provide power to the load or inject energy into the utility grid whenever required by the energy management strategy. The utility grid acts as an auxiliary energy source and can supply both the load demand and the battery storage system when local renewable generation is insufficient.

The power exchanged among the PV system, the battery storage system, and the utility grid is continuously coordinated by the EMS to ensure reliable operation and efficient utilization of available energy resources. Based

on the forecasted photovoltaic generation and load demand profiles, the EMS determines the optimal battery charging/discharging schedule and the optimal grid power exchange while satisfying all operational constraints.
To ensure the proper operation of the microgrid, the generated, stored, imported, exported, and consumed powers must satisfy the power balance condition at each scheduling interval. This energy balance principle constitutes the foundation of the EMS optimization framework developed in Section IV.
The following subsections present the mathematical models of the photovoltaic generation system, battery energy storage system, and utility grid interaction.

**C. Photovoltaic Generation Model**

The photovoltaic (PV) system is the microgrid's primary renewable energy source. Accurate modeling of its power output is essential for reliable forecasting and optimal energy management, as photovoltaic generation directly affects battery scheduling and grid power exchange decisions.
In this study, the photovoltaic power output is modeled using a simplified irradiance-based approach, which is widely adopted in energy management and scheduling applications due to its low computational complexity and satisfactory accuracy for system-level analysis. The generated PV power at time step t is expressed as:

$$\mathbf{P_{PV}(t) = \eta_{PV} A_{PV} G(t) * [1 - \gamma * (T(t) - T_{ref})]} \quad (1)$$

where:

- $P_{PV}(t)$ is the photovoltaic power output (kW);
- $\eta_{PV}$ is the nominal conversion efficiency of the PV modules;
- $A_{PV}$ is the total effective PV panel area ($m^2$);
- $G(t)$ is the solar irradiance ($W/m^2$);
- $T(t)$ is the ambient temperature ($°C$);
- $T_{ref}$ is the reference temperature under standard test conditions (25°C);
- $\gamma$ is the temperature coefficient of the PV module.

The first term of (2) represents the conversion of solar energy into electrical power as a function of the incident irradiance, while the second term accounts for the reduction in conversion efficiency caused by temperature variations. As the operating temperature increases, the PV module efficiency decreases, resulting in lower electrical power generation.
The generated photovoltaic power contributes directly to the microgrid energy balance and can be used to supply the local electrical load, charge the battery energy storage system, or export surplus energy to the utility grid according to the operating strategy determined by the Energy Management System (EMS).

**D. Battery Energy Storage Model**

The battery energy storage system (BESS) is integrated into the microgrid to enhance operational flexibility and mitigate the intermittent nature of photovoltaic generation. By storing excess renewable energy during periods of high PV production and releasing it when local generation is insufficient, the BESS contributes to improving energy self-consumption and reducing dependence on the utility grid.
Within the proposed EMS framework, the battery serves as the main flexibility resource and plays a central role in balancing power generation and demand. Depending on the operating conditions, the stored energy can be used to support the local load or to export energy to the utility grid when economically advantageous.
The battery operation is characterized by its state of charge (SOC), charging and discharging efficiencies, energy capacity, and power limits. These parameters determine the available storage capability and directly influence the energy scheduling decisions performed by the EMS.
The mathematical formulation governing the battery charging/discharging dynamics, SOC evolution, and operational constraints is presented in Section IV as part of the EMS optimization framework.

**E. Power Exchange with Utility Grid**

The utility grid provides an additional source of flexibility for the operation of the proposed microgrid. Through the grid interconnection, the microgrid can exchange energy with the main electrical network according to the operating conditions and the decisions generated by the Energy Management System (EMS).
When the local photovoltaic generation and battery resources are insufficient to satisfy the load demand, electrical energy can be imported from the utility grid to ensure uninterrupted power supply. Conversely, during periods of excess renewable generation or surplus stored energy, power can be exported to the utility grid, thereby improving the utilization of available energy resources.
The bidirectional power exchange capability contributes to enhancing the reliability and operational flexibility of the microgrid. It also allows the EMS to exploit variations in electricity tariffs by optimally coordinating battery scheduling and grid power transactions.
Within the proposed framework, the utility grid acts as both an auxiliary energy source and an energy sink, enabling the microgrid to maintain the balance between power generation, storage, and consumption under varying operating conditions.
The mathematical formulation governing the exchanged grid power and the associated operational constraints is presented in Section IV as part of the EMS optimization framework.

## III. DATA GENERATION AND BiLSTM FORECASTING MODEL

The operational efficiency of an intelligent Energy Management System (EMS) designed for industrial microgrids depends heavily on the accuracy of electrical load demand (P_load) and photovoltaic (PV) power (P_PV)

forecasting. Reliable predictions allow the central controller to anticipate severe industrial operating conditions and optimize multi-period scheduling strategies. In this work, a localized data-driven framework is developed through a multi-stage MATLAB simulation pipeline. The execution sequence systematically handles parameters specific to the industrial site of Hassi Messaoud, Algeria, moving from deterministic physical simulation to deep-learning-based temporal prediction. The global pipeline consists of three sequential stages: multi-variable data generation, statistical preprocessing, and BiLSTM neural network optimization.

**A. Industrial Data Generation and Site Modeling**

To rigorously evaluate the proposed EMS under real environmental constraints, the first stage of the MATLAB simulation synthesizes continuous time-series profiles emulating the microgrid state space of an industrial facility located in Hassi Messaoud. The generated multi-period dataset encompasses six concurrent variables :

$$X(t) = \left[ P_{load}(t), P_{PV}(t), G(t), T(t), H(t), C_{grid}(t) \right]^T \quad (2)$$

where $X(t)$ represents the multi-variable environmental-demand state vector at a discrete time step $t$. Within this state space:

- $P_{load}(t)$ denotes the instantaneous electrical load demand of the industrial facility $(kW)$;
- $P_{PV}(t)$ represents the output power generated by the photovoltaic array, measured in kilowatts $(kW)$;
- $G(t)$ is the global solar irradiance $(W/m^2)$;
- $T(t)$ corresponds is the ambient temperature $(°C)$;
- $H(t)$ denotes the relative humidity (%);
- $C_{grid}(t)$ represents the time-varying electricity price (€/kWh).

The superscript $T$ denotes the matrix transposition operator, indicating that $X(t)$ is mathematically structured as a $6 \times 1$ column vector to satisfy the input dimensionality requirements of the subsequent deep recurrent neural network.

The photovoltaic generation profiles used in this study were derived from the PV model presented in Section II-C and driven by realistic meteorological conditions representative of the Hassi Messaoud region. The generated dataset combines electrical, environmental, and economic variables required for both forecasting and energy management applications.

To assess the realism and seasonal consistency of the generated dataset, annual time-series profiles were produced for the year 2021. The resulting data capture the temporal variability of industrial load demand, photovoltaic generation, solar irradiance, ambient temperature, relative humidity, and electricity price. Fig. 2 illustrates the synthesized annual operating conditions of the considered industrial microgrid and provides a comprehensive visualization of the generated dataset.

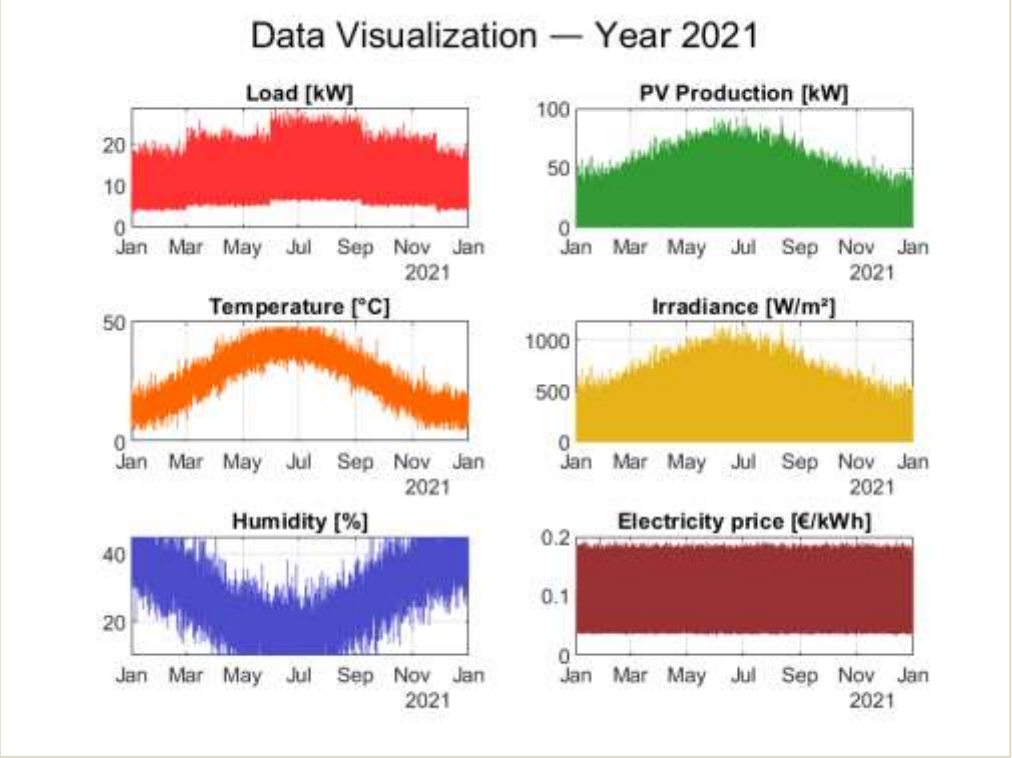



**Fig. 2. Simulated annual industrial electrical load profile and data visualization for the year 2021.**

**B. Data Preprocessing and Sequencing**

In the second simulation stage, raw synthesized variables are preprocessed within MATLAB to eliminate scaling bias across heterogeneous physical quantities and improve deep learning convergence. The preprocessing workflow involves noise filtering, sequential time-lag structuring, and Min-Max linear normalization. All variables are mapped into a dimensionless unified interval [0, 1] using the following transformation:

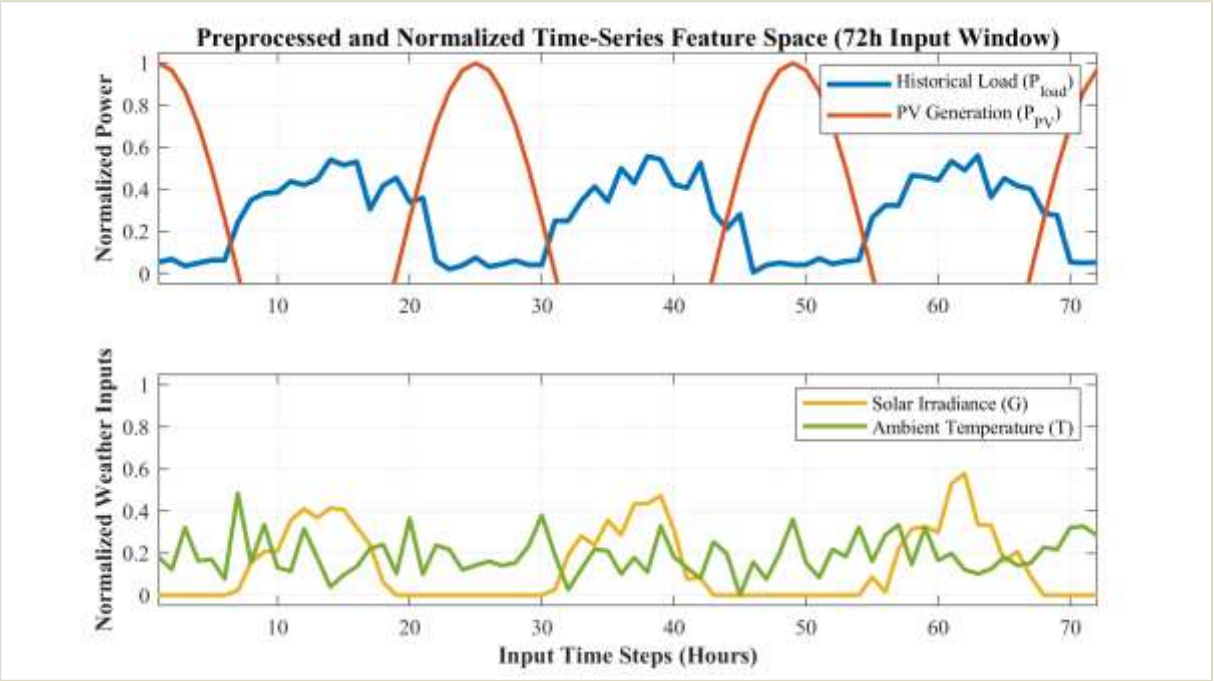
$$X_{norm} = \frac{(X - X_{min})}{(X_{max} - X_{min})}$$

where $X$ and $X_{norm}$ denote the raw and scaled industrial variables, respectively, while $X_{min}$ and $X_{max}$ represent the absolute boundaries observed across the historical horizon. The structured time-series matrix is then partitioned into a training subset ($X_{train}$) for gradient tuning and a validation subset (($X_{val}$) to evaluate generalization performance.

As observable from the 2021 dataset, the consumption peaks are predominantly concentrated during specific operational windows. To make these multi-variate profiles exploitable by the deep learning architecture, the raw time series are normalized, cyclically encoded, and structured into sliding windows (72-h input / 24-h prediction). The resulting preprocessed industrial feature space is illustrated in Fig. 3, where the upper subplot displays the bounded internal power variables ($P_{load} and\ P_{PV}$) and the lower subplot outlines the normalized environmental drivers ($G\ and\ T$).

Once this feature space is structured, these sequential matrices are partitioned into training and testing subsets to feed the proposed BiLSTM network.

**Fig. 3. Preprocessed and normalized industrial time-series feature space prepared for network training.**




### C. BiLSTM Forecasting Model Architecture

Standard unidirectional LSTM networks process sequential information only in the forward temporal direction, limiting their ability to exploit future contextual information. To capture temporal dependencies from both past and future observations simultaneously, a Bidirectional Long Short-Term Memory (BiLSTM) network is adopted in this work.

For a given input sequence $x_t$, each LSTM cell updates its hidden representation by processing the current input together with the information stored from previous time steps. The hidden state generated by a standard LSTM layer can be generally expressed as

$$h_t = LSTM(x_t, h_{t-1}, c_{t-1}) \quad (4)$$

where $x_t$ denotes the input vector, $h_t$ is the hidden state, and $c_{t-1}$ represents the memory cell state.

Within the BiLSTM architecture, two independent LSTM layers process the sequence in opposite temporal directions. The forward hidden state $h_f^t$ and backward hidden state $h_b^t$ are respectively computed as

$$h_f^t = LSTM_f(x_t, h_{t-1}^f) \quad (5)$$

$$h_b^t = LSTM_b(x_t, h_{t-1}^b) \quad (6)$$

The final bidirectional representation is obtained by concatenating both hidden states:

$$h_t = [h_f^t, h_b^t] \quad (7)$$

This bidirectional structure enables the network to exploit both historical and future contextual information, thereby improving the forecasting accuracy of photovoltaic generation and electrical load demand profiles.

The detailed architecture of the proposed BiLSTM forecasting model, including the configuration of each computational layer and its corresponding role within the forecasting framework, is summarized in Table I.

**TABLE I**: Computational Layer Configuration of the Proposed BiLSTM Network

| Layer Index | Layer Type | Output Shape / Hyperparameters | Function / Role in the Framework |
|---|---|---|---|
| **1** | **Sequence Input** | $6 \times 72$ | Accepts 6 physical/environmental variables over a 72-hour historical window. |
| **2** | **BiLSTM (Stacked 1)** | $64\ Hidden\ Units\ ('sequence')$ | Extracts forward and backward deep temporal context features across all time steps. |
| **3** | **Layer Normalization** | Channel-wise Normalization | Stabilizes gradient flow, prevents internal covariate shift, and accelerates training convergence. |
| **4** | **Dropout Regularization** | Regularization Rate = 0.2 | Prevents co-adaptation of weights and mitigates overfitting during training |
| **5** | **BiLSTM (Stacked 2)** | 32 Hidden Units ('last') | Captures the final consolidated hidden state vector at the last sequence step. |
| **6** | **Fully Connected** | 48 Linear Output Responses | Maps the extracted high-level features onto the multi-step prediction space. |
| **7** | **Regression Output** | $2 \times 24$ (Load & PV Trajectories) | Computes continuous loss residuals via RMSE during the optimization |

**D. Network Training and Performance Metrics**

The BiLSTM network parameters are optimized by minimizing prediction residuals via backpropagation through time. Core hyperparameters including the number of hidden units, initial learning rate, total training epochs, and mini-batch size are systematically tuned within the MATLAB script using grid search cross-validation. The prediction accuracy over the validation set D_val is quantified using Root Mean Square Error (RMSE) and Mean Absolute Error (MAE):

$$RMSE = \sqrt{\left[\left(\frac{1}{N}\right)\Sigma_{t=1}^{N}(y_t - \hat{y}_t)^2\right]}, \quad MAE = \left(\frac{1}{N}\right)\Sigma_{t=1}^{N}|y_t - \hat{y}_t|$$

Where $y_t$ and $\hat{y}_t$ represent the true measured and network-predicted industrial variables, respectively, and $N$ represents the total number of validation samples.

The training convergence and multi-step prediction performance of the proposed deep BiLSTM network are subsequently evaluated using the synthesized Hassi Messaoud dataset. As shown in Fig. 3, the network exhibits a highly stable and monotonic convergence within 30 epochs under the Adam optimizer, with the training RMSE dropping from over 3.5 to below 0.5 without any signs of overfitting.

Following this successful training phase, the model is validated on the test subset over a 24-hour horizon, displaying normalized profiles for both electrical demand and solar generation (Fig. 4). The model demonstrates exceptional tracking accuracy across the normalized scale, achieving a remarkably low mean test RMSE of 0.0631 for the industrial load demand and 0.0630 for the PV power output. Visually, the bidirectional architecture successfully captures the sharp morning and evening industrial load ramp-ups within the normalized boundaries. More importantly, the model accurately replicates the highly non-linear solar power drop observed at hour 8, effectively capturing sudden localized cloud coverage or irradiance intermittency on the normalized output curve. This high-fidelity forecasting framework provides reliable predictive trajectories to the downstream optimization layer, thereby mitigating microgrid operational uncertainties.

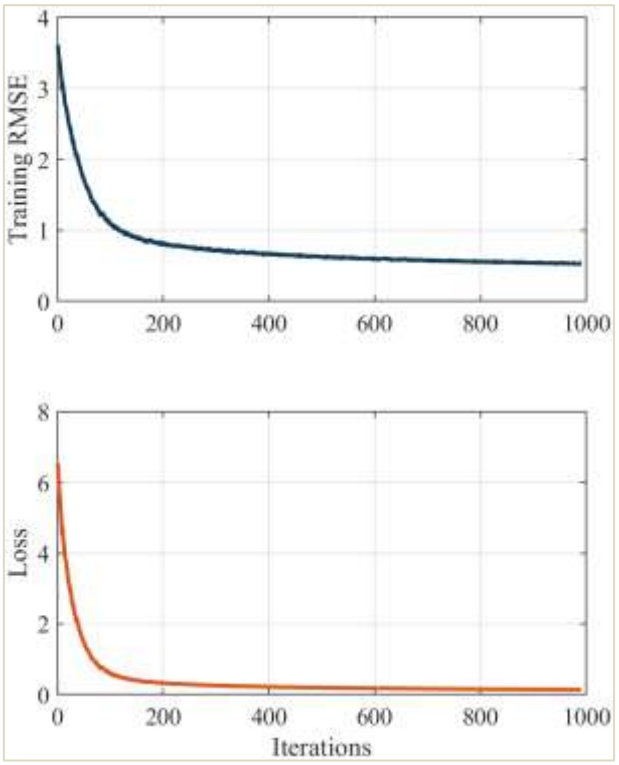



**Fig.4. Training Convergence**

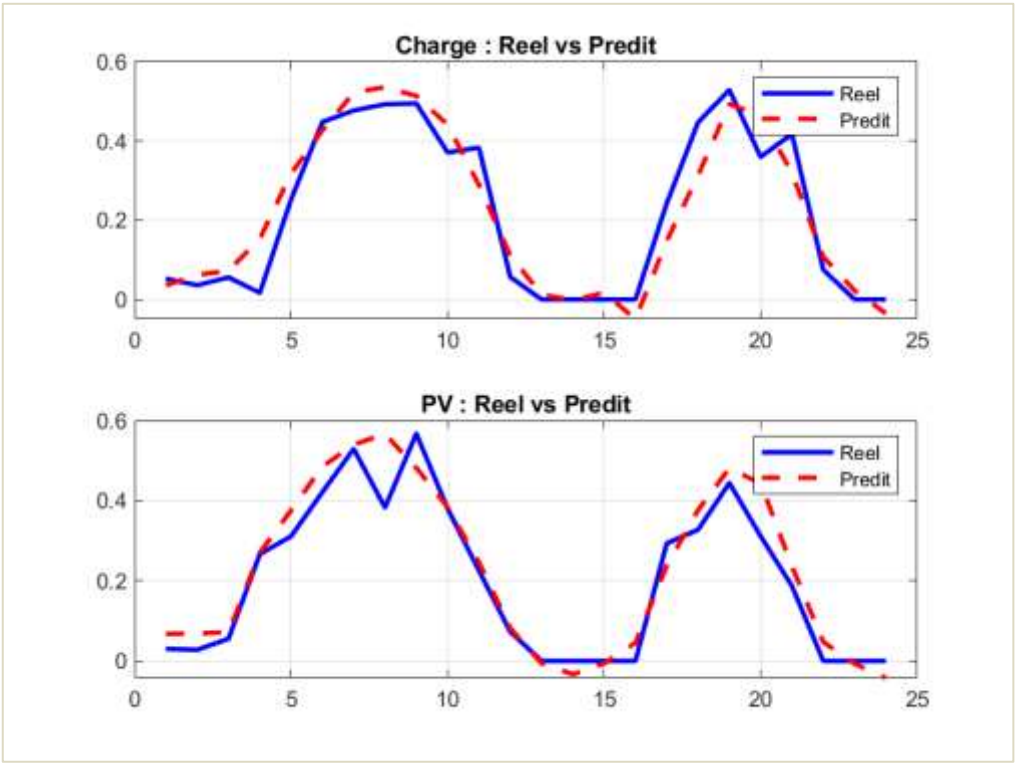



**Fig. 5. Comparison between real and predicted load demand and photovoltaic power generation profiles for Hassi Messaoud using the BiLSTM model.**

**E. Role of Forecasting in EMS Optimization**

The 24-hour ahead normalized predictive trajectories generated by the BiLSTM network specifically the predicted load demand $\hat{P}_{load}(t)$ and the estimated PV power generation $\hat{P}_{PV}(t)$ serve as critical deterministic parameters for the downstream optimization problem detailed in Section IV. Instead of relying on myopic or persistence-based forecasting methods, the proposed predictive stage injects these high-fidelity trajectories directly into the operational constraints of the Energy Management System (EMS). Mathematically, these profiles govern the state-of-charge $SOC$ dynamics of the central battery energy storage system $BESS$ and dictate the

optimal scheduling horizon by resolving the power balance equation at each hourly interval :

$$P_{grid}(t) + \widehat{P_{pv}}(t) + P_{batt,dis}(t) = \widehat{P_{load}}(t) + P_{batt,ch}(t) \quad (8)$$

By anticipating sharp industrial load peaks and localized daytime solar intermittency under extreme desert conditions, the optimization layer can proactively schedule battery charging cycles during high-generation windows and minimize expensive peak-hour power drawing from the utility grid $P_{grid}$ .Consequently, integrating this deep learning forecasting engine into the microgrid control framework establishes a robust bridge between temporal pattern recognition and real-time operational optimization, effectively maximizing renewable self-consumption while preserving battery health.

## IV. ENERGY MANAGEMENT SYSTEM FORMULATION

The proposed Energy Management System (EMS) aims to determine the optimal battery scheduling strategy using the load demand and photovoltaic generation forecasts provided by the BiLSTM model. The optimization process is performed over a 24-hour scheduling horizon and coordinates the interactions between the photovoltaic system, the battery energy storage system (BESS), and the utility grid.

**A. Power Balance Constraint**

The forecasted load demand and photovoltaic generation are first used to compute the net load:

$$P_{net}(t) = P_{load}^{pred}(t) - P_{PV}^{pred}(t) \quad (9)$$

where $P_{load}^{pred}(t)$ and $P_{PV}^{pred}(t)$ denote the forecasted load demand and photovoltaic generation, respectively.

The net load represents the residual electrical demand that must be supplied by the Battery Energy Storage System (BESS) and/or the utility grid after accounting for local photovoltaic generation.

To ensure reliable operation of the microgrid, the power balance equation must be satisfied at each scheduling interval:

$$P_{load}(t) = P_{PV}(t) + P_{grid}(t) + P_{bat}(t) \quad (10)$$

where:

- $P_{load}(t)$ is the load demand (kW);
- $P_{PV}(t)$ is the photovoltaic power generation (kW);
- $P_{bat}(t)$ is the battery charging/discharging power (kW);
- $P_{grid}(t)$ is the power exchanged with the utility grid (kW).

Using the net-load formulation, the exchanged grid power can be expressed as:

$$P_{grid}(t) = P_{net}(t) - P_{bat}(t) \quad (11)$$

which constitutes the fundamental EMS decision equation.

For optimization purposes, all internal energy exchanges within the microgrid are represented through the net grid power variable $P_{grid}(t)$ , which accounts for the combined effects of photovoltaic generation and battery scheduling decisions.

Although the physical microgrid enables multiple energy exchange paths between the PV system, the battery storage system, the load, and the utility grid, the EMS formulation captures these interactions through the battery power $P_{bat}(t)$) and the net grid power $P_{grid}(t)$). This representation simplifies the optimization problem while preserving the overall energy balance of the microgrid.

**B. Battery Energy Storage System Model**

The Battery Energy Storage System (BESS) is modeled through its State of Charge (SOC) dynamics.

$$SOC(t+1) = \begin{cases} SOC(t) - \dfrac{P_{batt}(t)\,\Delta t}{E_{bat}\,\eta_{dis}} & \text{if } P_{bat}(t) \geq 0 \quad (12) \\ SOC(t) - \dfrac{P_{bat}(t)\,\Delta t\,\eta_{ch}}{E_{bat}} & \text{if } P_{bat}(t) < 0 \quad (13) \end{cases}$$

where:

- $SOC(t)$ is the battery state of charge at time step $t$
- $E_{bat}$ is the nominal battery capacity (kWh)
- $\eta_{ch}$ is the charging efficiency
- $\eta_{dis}$ is the discharging efficiency
- $\Delta t$ is the sampling time interval (h)

To ensure safe operation and extend battery lifetime, the battery SOC is constrained by

$$SOC_{min} \leq SOC(t) \leq SOC_{max} \quad (14)$$

In addition, the battery charging and discharging power must satisfy

$$-P_{bat}^{max} \leq P_{bat}(t) \leq P_{bat}^{max} \quad (15)$$

These constraints prevent overcharging, deep discharging, and excessive battery utilization.

The battery model enables the EMS to optimally manage charging and discharging cycles in order to reduce grid dependency and improve overall economic performance.

**C Grid Power Constraints**

The power exchanged between the microgrid and the utility grid is represented by the variable $P_{grid}(t)$. Positive values of grid power indicate energy import from the main grid, while negative values correspond to energy export to the grid.

To ensure safe and stable operation of the grid connection, the exchanged power must remain within predefined technical limits:

$$P_{grid}^{min} \leq P_{grid}(t) \leq P_{grid}^{max}$$

where:

- $P_{grid}^{max}$ represents the maximum power that can be imported from the grid
- $P_{grid}^{min}$ represents the maximum power that can be exported to the grid

These limits are determined by technical characteristics of the grid connection and contractual agreements with the utility operator.

**D. Multi-Objective Optimization Problem**

The EMS optimization problem simultaneously minimizes electricity operating cost and battery degradation stress.

**1) Electricity Cost Objective**

The electricity cost objective is defined as:

$$J_1 = \sum_{t=1}^{N} C_{grid}(t)\, max(P_{grid}(t),0)\, \Delta t \quad (16)$$

where:

- $C_{grid}(t)$ represents the electricity price at time step $t$
- $P_{grid}(t)$ represents the power exchanged with the grid
- $\Delta t$ represents the sampling interval

The operator $max(P_{grid}(t),0)$ ensures that electricity cost is considered only when power is imported from the utility grid. Consequently, the EMS is encouraged to maximize the utilization of locally generated photovoltaic energy and stored battery energy.

**2) Battery Degradation Objective**

Frequent charging and discharging cycles accelerate battery aging and reduce its operational lifetime. Therefore, the second objective aims to limit battery degradation by penalizing both intensive battery utilization and abrupt power variations.

The battery degradation objective is formulated as

$$J_2 = \sum \left[\frac{P_{batt}(t)}{(P_{bat,max})^2}.\Delta t\right] + 0.1.\sum[|P_{bat}(t) - P_{bat}(t-1)|] \quad (17)$$

The first term penalizes excessive battery throughput, while the second term discourages rapid transitions between charging and discharging operating modes. This formulation promotes smoother battery operation and contributes to extending battery lifetime.

**3) Multi-Objective Formulation**

The optimization problem is therefore formulated as:

$Min\ F(X) = [J_1, J_2]$

Where $X = [P_{bat}(1), P_{bat}(2), \dots, P_{bat}(24)\ ]$

(18)

denotes the battery scheduling decision vector.

Since the two objectives are conflicting, the optimization process generates a set of Pareto-optimal solutions representing different trade-offs between electricity cost minimization and battery lifetime preservation.

**E. Constraint Handling and Optimization Variables**

To guarantee physically feasible operating conditions, constraint violations are incorporated into the objective functions through penalty terms.

The penalized objective functions are defined as

$$J_1^* = J_1 + Penalty_{SOC} + Penalty_{Grid} \quad (19)$$

$$J_2^* = J_2 + Penalty_{SOC} \quad (20)$$

Penalty terms are activated whenever SOC or grid-power limits are violated and are assigned sufficiently large coefficients to eliminate infeasible solutions from the search process.

The optimization vector is defined as:

$X = \{P_{bat}(1), P_{bat}(2), \dots, P_{bat}(N)\}$ subject to:

$P_{grid}^{min} \leq P_{grid}(t) \leq P_{grid}^{max}$

and the battery operational constraints defined in Section IV-B.

F. Comparative Multi-Objective Optimization Algorithms

Three multi-objective optimization algorithms are considered in this study: Non-dominated Sorting Genetic Algorithm II (NSGA-II), Multi-Objective Particle Swarm Optimization (MOPSO), and Adaptive Multi-Objective Particle Swarm Optimization (AMOPSO).

**1) NSGA-II**

NSGA-II is an evolutionary multi-objective optimization algorithm based on non-dominated sorting and crowding-distance mechanisms. It maintains population diversity while progressively approximating the Pareto-

optimal front. Candidate solutions are ranked according to dominance relationships and selection pressure is applied through elitist survival strategies.

**2) MOPSO**

MOPSO extends the conventional Particle Swarm Optimization algorithm to multi-objective problems by incorporating an external archive of non-dominated solutions. Particle movements are guided by Pareto leaders selected from the archive, allowing simultaneous exploration of multiple trade-off solutions.

**3) AMOPSO**

AMOPSO enhances the conventional MOPSO framework through adaptive parameter adjustment mechanisms that dynamically balance exploration and exploitation during the optimization process. This adaptive behavior improves convergence stability and helps maintain solution diversity across the Pareto front.

The three algorithms are employed to generate Pareto-optimal battery scheduling solutions that minimize electricity operating cost and battery degradation while satisfying all operational constraints. Their convergence characteristics, Pareto-front quality, and energy management performance are comparatively evaluated in Section V.

## V. RESULTS AND DISCUSSION

### A. Simulation Setup

The proposed EMS was implemented in MATLAB over a 24-h scheduling horizon using the photovoltaic power and load demand forecasts generated by the BiLSTM model. The optimization problem simultaneously minimizes electricity operating cost and battery cycling stress while satisfying battery SOC and grid operational constraints. NSGA-II, MOPSO, and AMOPSO were evaluated under identical conditions using the same population size and maximum number of iterations to ensure a fair comparison.

### B. Comparative Optimization Analysis

Fig. 6 compares the convergence behavior of the three optimization algorithms. MOPSO exhibits the fastest convergence and achieves the lowest objective value, demonstrating strong exploitation capability. In contrast, NSGA-II converges more gradually due to its stronger exploration mechanism, whereas AMOPSO presents intermediate behavior with smoother convergence characteristics.

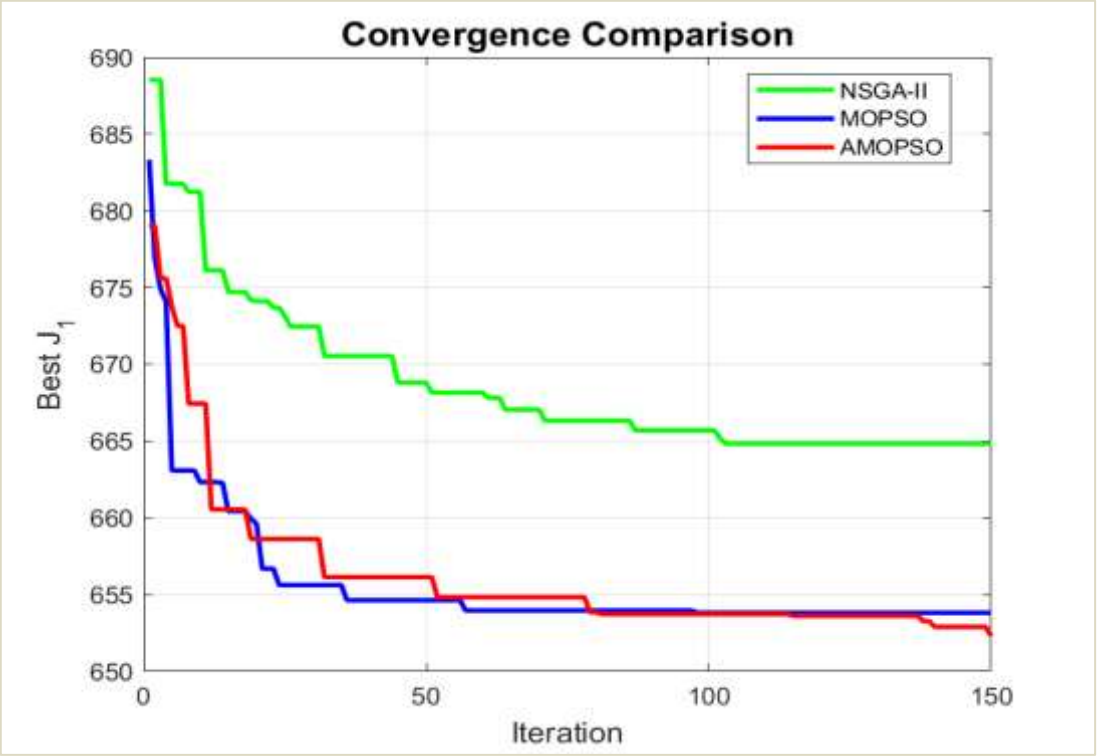
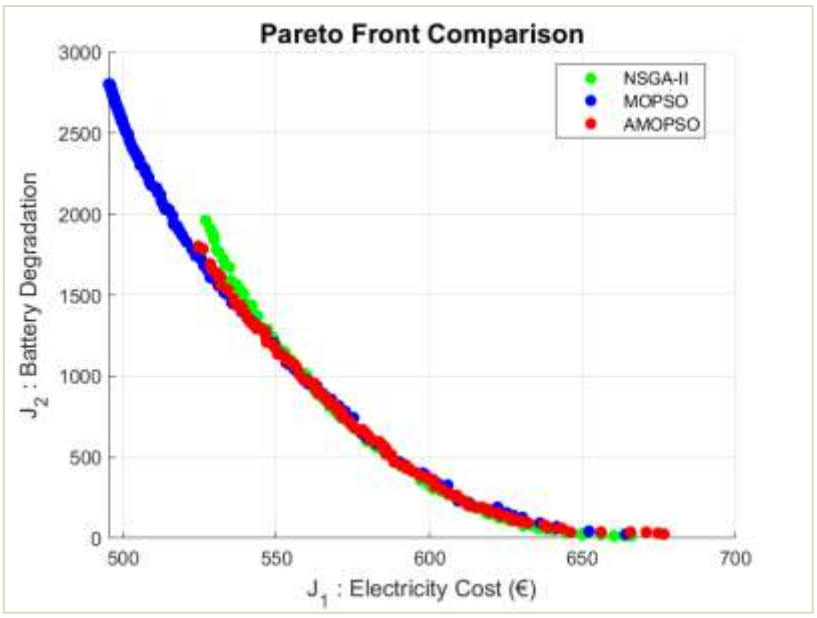



**Fig. 6.Convergence Comparison of NSGA-II, MOPSO, and AMOPSO**

The Pareto fronts shown in Fig. 7 illustrate the trade-off between operating electricity cost and battery cycling stress. NSGA-II provides a wider distribution of solutions, indicating superior exploration capability. MOPSO tends to concentrate solutions toward lower-cost regions, whereas AMOPSO generates compromise solutions between economic performance and battery utilization




.

**Fig.7 .Pareto Front Comparison of NSGA-II, MOPSO, and AMOPSO**

whereas AMOPSO generates compromise solutions between economic performance and battery utilization.

Table 2 summarizes the comparative performance metrics of NSGA-II, MOPSO, and AMOPSO. MOPSO achieves the lowest electricity operating cost (509.961 €) and best mean economic performance, demonstrating strong exploitation capability. However, it exhibits the highest battery stress indicator (Mean $J_2$ = 1045.011), reflecting more intensive battery utilization. In contrast, NSGA-II provides the highest diversity (22.851) and hypervolume (1.231), indicating superior Pareto-front exploration and solution diversity. AMOPSO offers a balanced compromise, maintaining competitive operating costs while achieving the lowest mean battery stress indicator (593.557) and the best spread (0.807) with highly stable convergence. These results confirm that each algorithm presents distinct trade-offs between economic performance, battery cycling effort, and search diversity.

**TABLE 2: Comparative Performance Metrics of Multi-Objective Optimization Algorithms**

| Algorithm | Min $J_1$ (€) | Mean $J_1$ (€) | Min $J_2$ | Mean $J_2$ | Diversity | Spread | Hypervolume | Stability |
|---|---|---|---|---|---|---|---|---|
| NSGA-II | 529.565 | 589.008 | 2.785 | 692.722 | **22.851** | 0.426 | **1.231** | 2.151 |
| MOPSO | **509.961** | **570.074** | 6.093 | 1045.011 | 12.491 | 0.726 | 1.168 | 0.291 |
| AMOPSO | 521.956 | 593.066 | 5.264 | **593.557** | 12.745 | **0.807** | 1.195 | **0.000** |

**C. Operational Analysis of the Energy Management System**

The optimal battery scheduling profile is illustrated in Fig 8. The battery is primarily charged during periods of low prices and discharged during periods of high prices, thus demonstrating the ability of the EMS system to exploit variations in electricity prices while limiting excessive battery charge/discharge cycles.

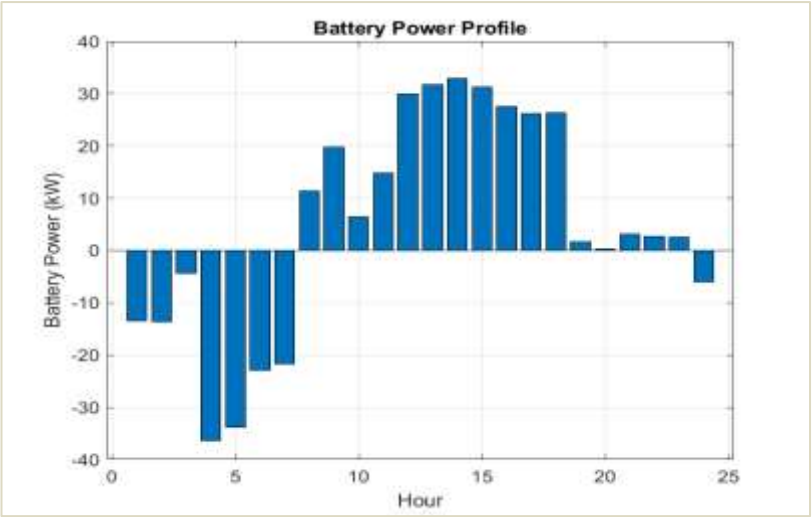



**Fig.8.Battery Power Profile**

The corresponding grid power profile, illustrated in Fig.9, indicates reduced grid dependence during periods of battery backup and photovoltaic production. Therefore, the energy management system (EMS) improves local energy utilization while maintaining power balance within the microgrid.

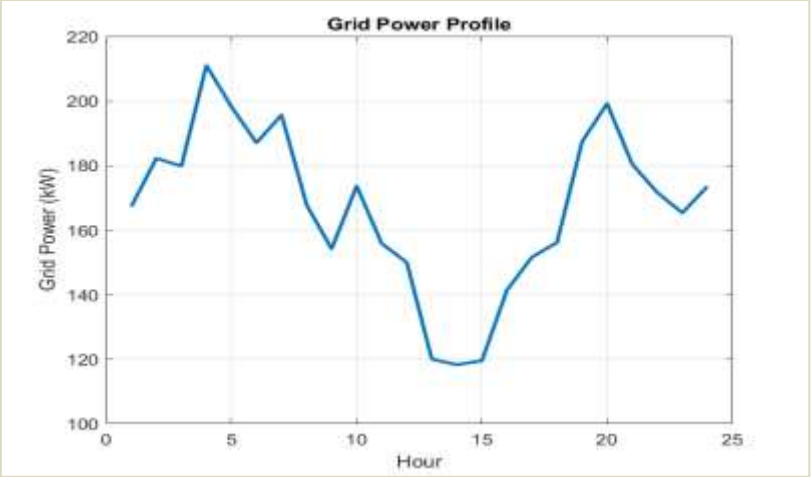



**Fig.9. Grid Power Profile**

The SOC evolution illustrated in Fig. 10 confirms that battery operation remains within the prescribed limits throughout the scheduling horizon. The SOC trajectory reflects efficient battery utilization while ensuring operational safety and constraint satisfaction.

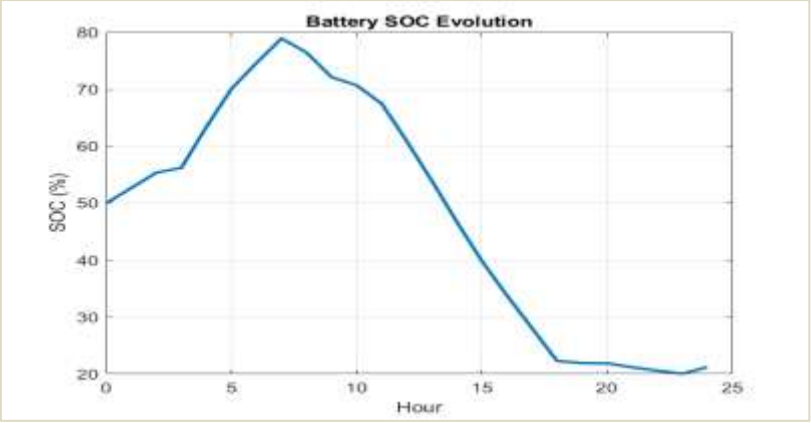



**Fig.10. Battery SOC Evolution**

The relationship between electricity prices and battery management is illustrated in Fig 11. Charging periods coincide with periods of low electricity prices, while discharging occurs during periods of high prices. This behavior confirms the energy management system's ability to optimize energy planning based on economic needs.

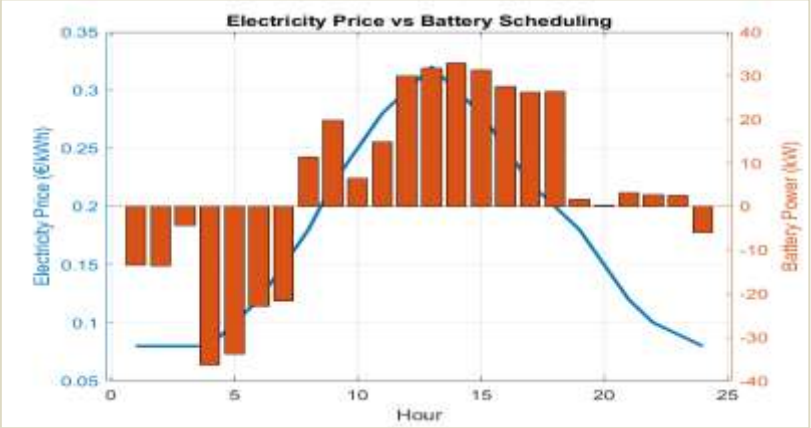



**Fig.11. Electricity Price vs Battery Scheduling**

**D. Discussion**

The comparative analysis demonstrates that no optimization algorithm surpasses all performance criteria. MOPSO offers the best economic performance, NSGA-II a greater diversity of solutions, and AMOPSO generates

balanced trade-offs between electricity cost and battery utilization. Overall, the combination of BiLSTM forecasting and multi-objective optimization provides an effective framework for intelligent energy management of grid-connected microgrids.

## VI. Conclusion

This paper presented a comparative multi-objective optimization framework for intelligent energy management of a grid-connected microgrid using BiLSTM forecasting and advanced swarm intelligence optimization techniques.

The proposed Energy Management System (EMS) integrates photovoltaic generation, battery energy storage, and bidirectional grid interaction in order to improve the economic and operational performance of the microgrid. Accurate forecasting of load demand and photovoltaic power generation was achieved using a Bidirectional Long Short-Term Memory (BiLSTM) neural network, which demonstrated strong capability in modeling the nonlinear temporal behavior of both renewable generation and electricity demand.

A multi-objective optimization problem was formulated over a 24-hour scheduling horizon to simultaneously minimize electricity operating cost and battery degradation. The optimization process determines the optimal battery charging and discharging scheduling strategy while satisfying the operational constraints of the microgrid, including battery State of Charge (SOC) limits and grid power constraints.

To evaluate the effectiveness of the proposed EMS framework, a comparative analysis involving NSGA-II, MOPSO, and the proposed Adaptive Multi-Objective Particle Swarm Optimization (AMOPSO) algorithm was conducted. The obtained results demonstrated different optimization behaviors among the considered approaches.

MOPSO achieved the lowest electricity operating cost due to its strong exploitation capability. However, this aggressive optimization behavior resulted in higher battery utilization and increased battery degradation. NSGA-II provided better Pareto front diversity and exploration capability, although with slower convergence behavior.

The proposed AMOPSO achieved a more balanced trade-off between economic performance and battery lifetime preservation. The adaptive optimization mechanisms improved convergence stability while maintaining competitive electricity cost minimization performance and reducing excessive battery utilization. Furthermore, the operational analysis confirmed the capability of the proposed EMS to intelligently coordinate battery scheduling and grid interaction according to electricity price variations and renewable energy availability.

Overall, the obtained results demonstrate that the integration of BiLSTM forecasting with adaptive multi-objective optimization provides an effective and practical solution for intelligent energy management in grid-connected microgrids. The proposed framework contributes to improving energy scheduling reliability, battery utilization efficiency, and operational flexibility in modern smart grid applications.

Future work may include the integration of electric vehicles, demand response strategies, uncertainty modeling, and real-time implementation of the proposed EMS under dynamic operating conditions. In addition, advanced deep learning architectures and stochastic optimization techniques may be investigated to further enhance forecasting accuracy and system robustness.

## Reference

[1] M. Uddin, H. Mo, D. Dong, S. Elsawah, J. Zhu, and J. M. Guerrero, "Microgrids: A review, outstanding issues and future trends," Energy Strategy Reviews, vol. 49, p. 101127, 2023. doi: 10.1016/j.esr.2023.101127.

[2] M. Abbasi, E. Abbasi, L. Li, R. P. Aguilera, D. Lu, and F. Wang, "Review on the microgrid concept, structures, components, communication systems, and control methods," Energies, vol. 16, no. 1, p. 484, 2023. doi: 10.3390/en16010484.

[3] S. E. Eyimaya and N. Altin, "Review of Energy Management Systems in Microgrids," Applied Sciences, vol. 14, no. 3, Art. no. 1249, 2024, doi: 10.3390/app14031249.

[4] F. Agha Kassab, R. Rodríguez Velásquez, B. Celik, F. Locment, and M. Sechilariu, "A Comprehensive Review of Sizing and Energy Management Strategies for Optimal Planning of Microgrids with PV and Other Renewable Integration," Applied Sciences, vol. 14, no. 22, Art. no. 10479, 2024, doi: 10.3390/app142210479.

[5] A. Dev, V. Kumar, G. Khare, J. Giri, M. Amir, F. Ahmad, P. Jain, and S. Anand, "Advancements and challenges in microgrid technology: A comprehensive review of control strategies, emerging technologies, and future directions," Energy Science & Engineering, 2025. doi: 10.1002/ese3.2095.

[6] S. T. Saranya and P. Bhowmik, "A comprehensive review of microgrid architectures, power management and resilient operation", Energy Reports, vol. 15, Art. 109021, 2026, doi: 10.1016/j.egyr.2025.109021.

[7] N. Khosravi, D. Çelik, H. Bevrani, and S. Echalih, "Microgrid Stability: A Comprehensive Review of Challenges, Trends, and Emerging Solutions," Int. J. Electr. Power Energy Syst., vol. 170, Art. 110829, 2025, doi: 10.1016/j.ijepes.2025.110829.

[8] A. Joshi, S. Capezza, A. Alhaji, and M.-Y. Chow, "Survey on AI and Machine Learning Techniques for Microgrid Energy Management Systems," IEEE/CAA Journal of Automatica Sinica, vol. 10, no. 7, pp. 1513–1529, 2023, doi: 10.1109/JAS.2023.123657.

[9] C. O. Egbuna et al., "Advances in AI-powered energy management systems for renewable-integrated smart grids," World J. Adv. Eng. Technol. Sci., vol. 15, no. 2, pp. 2300–2325, 2025, doi: 10.30574/wjaets.2025.15.2.0685.

[10] D. Razmi, P. Razmi, O. Babayomi, and Z. Zhang, "Toward intelligent and resilient microgrids: A survey of machine learning approaches for renewable energy integration," Applied Energy, vol. 415, p. 127929, 2026, doi: 10.1016/j.apenergy.2026.127929.
[11] S. Nazaralizadeh, P. Banerjee, A. K. Srivastava, and P. Famouri, "Battery Energy Storage Systems: A Review of Energy Management Systems and Health Metrics," Energies, vol. 17, no. 5, Art. 1250, 2024. doi: 10.3390/en17051250.
[12] N. Shamarova, K. Suslov, P. Ilyushin, and I. Shushpanov, "Review of battery energy storage systems modeling in microgrids with renewables considering battery degradation," Energies, vol. 15, no. 19, p. 6967, 2022. doi: 10.3390/en15196967.
[13] A. Bensalem, B. Toual, M. Elbar, M. Khaleel, and Z. Belboul, "A framework to quantify battery degradation in residential microgrid operate with maximum self-consumption based energy management system," Studies in Engineering and Exact Sciences, 2024. doi: 10.54021/seesv5n2-026.
[14] X. Dai and K. Batool, "Optimizing multi-objective design, planning, and operation for sustainable energy sharing districts considering electrochemical battery longevity," Journal of Energy Storage, vol. 96, p. 112550, 2024. doi: 10.1016/j.est.2024.112550.
[15] K. H. Ali, M. Abusara, A. A. Tahir, and S. Das, "Dual-layer Q-learning strategy for energy management of battery storage in grid-connected microgrids," Energies, vol. 16, p. 1334, 2023, doi: 10.3390/en16031334.
[16] G. S. Thirunavukkarasu et al., "Role of optimization techniques in microgrid energy management systems — a review," Energy Strategy Reviews, vol. 43, 2022, doi: 10.1016/j.esr.2022.100899.
[17] N. Salehi, H. Martinez-Garcia, G. Velasco-Quesada, and J. M. Guerrero, "A comprehensive review of control strategies and optimization methods for individual and community microgrids," IEEE Access, vol. 10, pp. 15935–15969, 2022, doi: 10.1109/ACCESS.2022.3142354.
[18] M. Brahmankar and C. -I. Chen, "Comparative Analysis of GA and NSGA-II for Multi-Objective Energy Management: Cost, Battery Degradation, and Renewable Utilization," 2025 Seventh International Symposium on Computer, Consumer and Control (IS3C), Taichung, Taiwan, 2025, pp. 1-5, doi: 10.1109/IS3C65361.2025.11131087.
[19] P. Horrillo-Quintero et al., "Adaptive multi-objective real-time hierarchical control for isolated microgrid clusters utilizing an enhanced particle swarm optimization strategy to optimize costs and emissions", Electric Power Systems Research, vol. 250, p. 112169, Jan. 2026, doi: 10.1016/j.epsr.2025.112169.
[20] S. Islam, S. Mostaghim, and M. Hartmann, "A survey on multi-objective optimization in microgrid systems," in IEEE Congress on Evolutionary Computation (CEC), Yokohama, Japan, 2024, pp. 1-8.
[21] G. L. do Nascimento Silva et al., "A comprehensive review of sizing and energy management strategies for optimal planning of microgrids with PV and other renewable integration," Applied Sciences, vol. 14, no. 22, Art. no. 10479, 2024, doi: 10.3390/app14221047.
[22] D. Yu and J. Liu, "Deep learning for renewable energy forecasting: A taxonomy and systematic literature review," Journal of Cleaner Production, vol. 384, p. 135414, 2023, doi: 10.1016/j.jclepro.2022.135414.
[23] M. Abou Houran, S. M. S. Bukhari, M. H. Zafar, M. Mansoor, and W. Chen, "COA-CNN-LSTM: Coati optimization algorithm-based hybrid deep learning model for PV/wind power forecasting in smart grid applications," Applied Energy, vol. 349, p. 121638, 2023, doi: 10.1016/j.apenergy.2023.121638.
[24] A. Agga, A. Abbou, M. Labbadi, Y. El Houm, and I. H. O. Ali, "CNN-LSTM: An efficient hybrid deep learning architecture for predicting short-term photovoltaic power production," Electric Power Systems Research, vol. 208, p. 107908, 2022, doi: 10.1016/j.epsr.2022.107908.
[25] M. A. Bou-Rabee, M. Y. Naz, I. E. Albalaa, and S. A. Sulaiman, "BiLSTM network-based approach for solar irradiance forecasting in continental climate zones," Energies, vol. 15, no. 6, p. 2226, 2022. doi: 10.3390/en15062226.
[26] A. Zameer, F. Jaffar, F. Shahid, M. Muneeb, R. Khan, and R. Nasir, "Short-term solar energy forecasting: Integrated computational intelligence of LSTMs and GRU," PLOS ONE, 2023, doi: 10.1371/journal.pone.0285410.
[27] F. Moazzen et al., "Multivariate deep learning long short-term memory forecasting for day-ahead energy management in microgrids," Energies, vol. 17, no. 17, 2024, doi: 10.3390/en17174237.
[28] M. N. Akhter, S. Mekhilef, H. Mokhlis et al., "An hour-ahead PV power forecasting method based on an RNN-LSTM model for three different PV plants," Energies, vol. 15, no. 6, p. 2243, 2022, doi: 10.3390/en15062243.
[29] N. Mounir, H. Ouadi, and I. Jrhilifa, "Short-term electric load forecasting using an EMD-BiLSTM approach for smart grid energy management system," Energy and Buildings, vol. 288, p. 113022, 2023, doi: 10.1016/j.enbuild.2023.113022.
[30] Y. Wang, W. Jiang, C. Wang, Q. Song, T. Zhang, Q. Dong, and X. Li, "An electricity load forecasting model based on multilayer dilated LSTM network and attention mechanism," Frontiers in Energy Research, vol. 11, p. 1116465, 2023, doi: 10.3389/fenrg.2023.1116465.
[31] C. Pavlatos et al., "Enhancing electrical load prediction using a bidirectional LSTM neural network," Electronics, vol. 12, no. 22, p. 4652, 2023, doi: 10.3390/electronics12224652.
[32] H. Shi, K. Miao, and X. Ren, "Short-term load forecasting based on CNN-BiLSTM with Bayesian optimization and attention mechanism," Concurrency and Computation: Practice and Experience, vol. 35, no. 17, p. e6676, 2023, doi: 10.1002/cpe.6676.

[33] Benameur, K., Mouchaal, Y., Benchouk, K., Laafer, A., & Barille, R. (2022). Synthesized and characterizations nanoparticles of chalcopyrite alloy CuIn1-xFexSe2. Inorganic Chemistry Communications, 136, 109165. https://doi.org/10.1016/j.inoche.2021.10916

[34] Foual, M., Sad Chemloul, N. E., Chaib, K., Abdellatif, H. E., Fellague Chebra, et al. (2024). Comparative analysis of tube designs in heat exchangers: A numerical simulation study for enhanced thermal-flow efficiency," optimizing wavy tubes bundle geometries for enhanced heat transfer in underwater applications". Numerical Heat Transfer, Part A: Applications, 87(1), 2369943. https://doi.org/10.1080/10407782.2024.2369943

[35] Hmida, A., Erchiqui, F., Laafer, A., & Bourouis, M. (2025). Energy Efficiency in Buildings Through the Application of Phase Change Materials: An In-Depth Analysis of the Integration of Spent Coffee Grounds (SCGs). Energies, 18(14), 3629. https://doi.org/10.3390/en18143629